JOURNAL OF CATALYSIS 89, 348–361 (1984)

FTIR Studies of Surface Reaction Dynamics

I. Temperature and Concentration Programming during CO Oxidation on Pt/SiO_2

DAVID J. KAUL AND EDUARDO E. WOLF[1]

Chemical Engineering Department, University of Notre Dame, Notre Dame, Indiana 46556

Received September 22, 1983; revised May 24, 1984

A transient technique integrating FTIR spectroscopy with Temperature-Programmed Reaction (TPR) and Concentration-Programmed Reaction (CPR) using a small-volume infrared reactor, has been developed. Studies of CO oxidation on a Pt/SiO_2 catalyst using these methods, have shown the occurrence of remarkable surface temperature behavior in regions of ignition and quenching. Extensive documentation of linear-bonded CO behavior is presented and the relevance of a Langmuir–Hinshelwood and other reaction models is discussed. Two different energy transport mechanisms are described which might lead to the observed catalyst temperature excursions.

INTRODUCTION

In recent years infrared spectroscopy (ir) has become a mature tool to study adsorbed species on supported metal catalysts (*1–4*). Similarly, the use of transient techniques in catalysis has grown as researchers discovered the wealth of information contained in this type of experimentation (*5–7*). Transient ir experiments permit us to follow dynamic behavior of surface intermediates, thus providing information concerning the nature of elementary steps which underlie the observed kinetics but cannot be unveiled by steady-state experiments. Today, transient ir measurements are possible with the use of fast ir spectrometers now commercially available along with specially designed small-volume reactors (*8–11*). Fourier Transform Infrared Spectroscopy (FTIR) is particularly suited for transient studies on supported catalysts since it provides full high-resolution spectra faster than dispersive instruments (Fellgett's advantage) and high ir throughput (Jacquinot's advantage). In this paper we report results obtained with a novel infrared reactor system having capabilities for temperature and concentration programming. The small-volume infrared cell reactor incorporates optimum characteristics of previous designs (*8, 9*) along with our own refinements for simultaneous measurement of surface and gas-phase temperatures. Computerized FTIR data acquisition and supporting software are used along with programming of the input variables in order to develop a fully integrated transient technique for Temperature-Programmed Reaction (TPR) and Concentration-Programmed Reaction (CPR) experiments.

We chose to study the oxidation of carbon monoxide because of its practical importance and apparent relative simplicity. Although extensive theoretical and experimental efforts have been dedicated to the study of this reaction, some recent review articles (*12, 13*) emphasize the lack of a quantitative understanding regarding its dynamic behavior. The use of comprehensive surface measurements and transient techniques such as developed in this work is still required to provide a basis for sound new mechanistic inferences. Our results

[1] To whom correspondence should be addressed.

0021-9517/84 $3.00

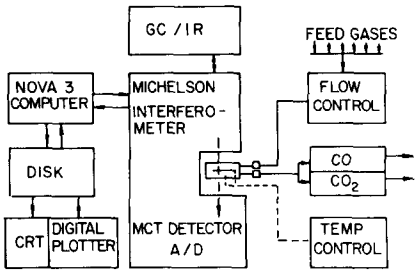

FIG. 1. Schematic of the experimental apparatus. The reactor and heater assembly are fully accommodated within the purged environment of the spectrometer sample chamber to intercept the infrared beam.

have uncovered evidence for an important heat transport mechanism in supported catalysts which cannot easily be explained. We also document the behavior of linear-bonded CO over a wide temperature and concentration range of dynamic behavior. These results provide new insight concerning the true kinetic role of this reaction intermediate.

EXPERIMENTAL

1. Infrared spectrometer. A schematic of the spectrometer and auxilliary apparatus is shown in Fig. 1. The infrared system used in our laboratory is a Digilab FTS-15C Fourier transform infrared spectrometer capable of 0.25 wavenumber resolution. A liquid-nitrogen-cooled Hg–Cd–Telluride detector provides for high-speed, high-sensitivity data acquisition by a Nova 3 minicomputer having a 5-megabyte hard disk data storage capability. A high-intensity copper glow bar source provides strong infrared throughput and thus allows adequate signal-to-noise ratio to be obtained in a single spectral scan. The operation of the instrument at 8 wavenumber resolution provides reproducible single-scan data in an average of 1 s during transient experiments. Prior to each experiment, a single-beam reference spectrum of the freshly reduced catalyst disk is recorded digitally. Subsequent single-beam spectra are recorded with reaction taking place at the catalyst surface. These spectra are ratioed against the stored reference spectrum of the bare surface to eliminate absorption by the catalyst support and any other background absorption.

Special software has been developed by Digilab for GC–IR experiments, i.e., gas chromatographic (GC) separation followed by ir identification of the emerging GC peaks. Such software is especially suited for transient kinetic experiments as well. Infrared spectra can be recorded in successive scan sets, each containing a user-specified number of co-added spectra. The data acquisition is clocked and real time is recorded for each scan set. The total number of scan sets is limited only by the available disk space (we have recorded up to 18,000 spectra in sets of 10 co-added scans during a single 5-h experiment). After collection, baseline-corrected absorbance peak height in a specified frequency range can be monitored as a function of real time using our own modified version of the GC software. The frequency of the absorbance maximum is also monitored. The data is then plotted as a spectragram (absorbance vs time) or a wavegram (frequency vs time). The ir results in this paper are presented in the above form rather than as individual spectra.

2. Reactor system. The reactor body (Fig. 2a) is constructed from a pair of blank Varian 2.75-in. stainless-steel Conflat flanges in a fashion similar to that described by Hegedus (*8*). These flanges are machined to create a reaction chamber encircled by a sharp-edged surface on each half. These surfaces are compressed by six Allen bolts against an aluminum gasket to form a leak-free seal. Gas inlet and outlet ports as well as two thermocouple ports are bored into the reaction chamber as shown in Fig. 2a. Sapphire windows brazed into Kovar sleeves (EIMAC) were welded into 13.6-mm holes at the center of each of the conflat flanges. This allows infrared transmission from 20,000 to 1400 cm^{-1} (*6*) and safe operation to 500°C.

The catalyst sample holder (Fig. 2b) consists of wafer support and retainer portions

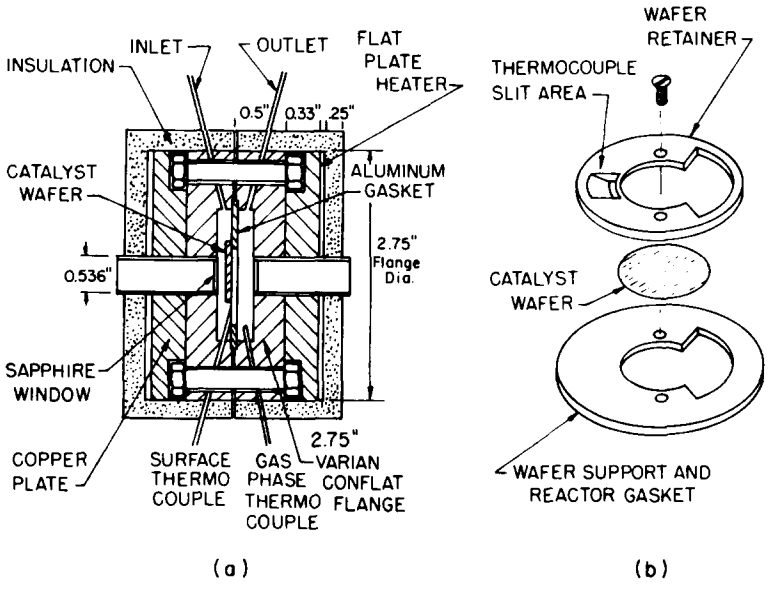

FIG. 2. Schematic of the infrared cell reactor. (a) Details of the inlet and outlet flows, thermocouples, and the infrared windows are shown in relation to the mounted catalyst wafer; (b) design of the catalyst wafer holder showing the slit which guides the foil thermocouple onto the catalyst surface during mounting.

which are held together with stainless-steel screws. A catalyst wafer of about 2 cm in diameter can be sandwiched between these parts with little chance of breakage and thus firmly supported in the path of the infrared radiation. The cutaway portion of the holder is positioned opposite the inlet and outlet ports so that the gases must sweep both sides of the catalyst wafer while passing through the reactor. The wafer support also serves as the aluminum gasket for the reactor. The small portion of the holder contains a groove and slit which serves to guide and hold a foil Omega Cement-On, Style II, Chromel–Alumel thermocouple directly onto the catalyst surface. The foil leads are spot-welded to a standard 0.062-in.-diameter Omegaclad thermocouple wire. This is fed through a $\frac{1}{16}$-in. Swagelok tube fitting to seal the reactor. To insure that the thermocouple leads are insulated from the aluminum disk holder, Omega CC high-temperature porcelain cement is applied to the grooved area. During assembly of the reactor, the thermocouple is guided through the slit as the disk holder is being positioned between the flanges. When in place, the delicate junction is just in view at the perimeter of the window, yet does not interfere with the infrared throughput. Contact with the catalyst surface is maintained by the thermocouple's own rigidity, rather than through the use of an adhesive which might interfere with the catalyst activity. Once the thermocouple has been positioned in this manner, its rapid response time (5 ms) allows precise monitoring of the catalyst wafer temperature during reaction transients.

Gas-phase temperature is monitored by an Omega Chromel–Alumel quick-disconnect thermocouple assembly, fed through a second $\frac{1}{16}$-in. Swagelok tube fitting. This thermocouple signal provides feedback to an Omega digital proportional controller for set-point control of the reaction temperature or to a TECO TP-2000 temperature programmer for TPR studies. To provide a stable source of feedback, the end of the thermocouple is positioned flush with the

reactor wall. Thus, we are essentially controlling the reactor with the wall temperature rather than using a bulk gas temperature near the catalyst where large fluctuations are likely to occur.

The reactor assembly is heated by two Chromalox, Type A, 120-V, 200-W, ring heaters manufactured by Tourtelot Company, providing heating in excess of 400°C. One-centimeter-thick copper plates are placed between each heater and the face of the reactor flange to insure uniform heating. The entire system is insulated in a two-part mold of ceramic fiber insulation supported with refractory cement.

The gas ports from the reactor are connected directly to a pair of 3-way valves which allow rapid switching to bypass the reactor. This enables continuous flow or batch reactor operation as well as the ability to isolate the reactor after a pretreatment step while allowing reactant concentrations to come to steady state in the feed gas mixture. Beyond the 3-way valves, each $\frac{1}{8}$-in. tube terminates in a Swagelok miniature quick-connect to enable the complete reactor assembly to be disconnected and removed from the spectrometer without exposing the catalyst to the atmosphere. The entire reactor assembly is supported in the sample chamber of the spectrometer from a flat stainless-steel plate.

The reactant gases, CO, O_2, and N_2 pass through a PFD mass flow controller before entering a manifold where they are mixed to the desired feed composition. An R.C. control circuit of our own design can be connected into either of the channels of the mass flow controller. This enables concentration programming at any desired rate and between any desired range of concentrations. A 4-way switching valve enables step changes to pure inert carrier gas during desorption experiments. Another 4-way valve allows selection of other gases including H_2, He, and calibration gases for CO and CO_2. The gas phase leaving the reactor is sent to a pair of Beckman ir analyzers for precise monitoring of gas-phase CO and CO_2 concentration. Ultrahigh purity H_2 and N_2 (Linde) are used along with zero grade O_2 and either research grade or CP grade CO. The nitrogen is passed through a zeolite water trap before mixing with other reactants. The CO is further purified in a cold molecular sieve trap to remove possible iron carbonyls.

TABLE 1

Catalyst Properties

Support	SiO_2 (Harshaw)
Preparation	H_2PtCl_6 Impregnation
Pt (wt%)	5.0
Pt Dispersion[a] (%)	16.9
Crystallite size[a] (Å)	68
BET area[b] (m^2/g)	590
Pore size distribution[b] (%)	
<120 Å	61.8
120–5.2 Å	15.2
>5.2 Å	23.0
Wafer characteristics[c]	
Av diameter (cm)	2.3
Av thickness (cm)	0.01
Av weight (g)	0.027
ρ_s (g/cm^3)	3.59
ρ_p (g/cm^3)	0.65
a (cm^2 Pt/cm^3 wafer)	11.1×10^4

[a] Determined by CO chemisorption.

[b] Manufacturer's analysis.

[c] Formed from the dried impregnated powder by compressing at 10,000 lb/in^2.

3. Catalyst properties. The current CO oxidation studies were performed over a 5 wt% Pt/SiO_2 catalyst. The catalyst sample was prepared by incipient wetness impregnation of silica gel (Harshaw) with a solution of chloroplatinic acid of the desired composition. After drying, the catalyst was oxidized in a flow reactor for 4 h at 350°C and then reduced for 8 h at 350°C. A catalyst disk 2.2 cm in diameter and 0.1-mm thick was pressed from 0.03 g of catalyst under a pressure of 10,000 lb in^{-2}. The wafer was again reduced *in situ* in the ir reactor for 2 h at 200°C preceding each run. The catalyst properties and wafer characteristics are summarized in Table 1.

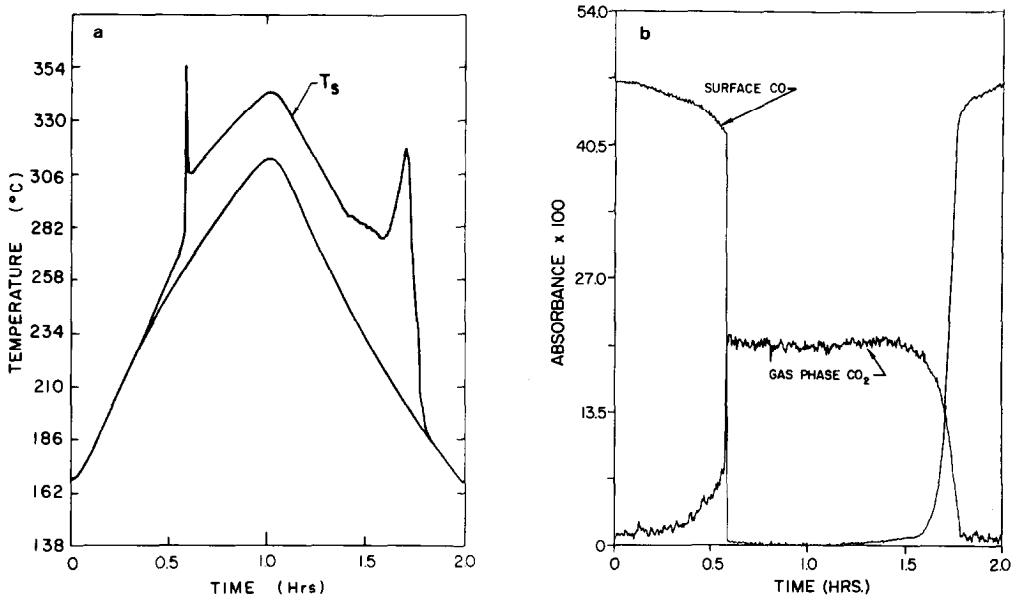

FIG. 3. Temperature ramp with constant inlet flows of 220 cm^3/min N_2, 9 cm^3/min CO, and 5 cm^3/min O_2. (a) The input ramp and the resultant surface temperature; (b) infrared spectragrams of the *in situ* CO_2 absorbance response and the linear-bonded CO surface species.

RESULTS

One of the characteristics of the transient techniques is the ability to obtain a substantially greater amount of data than by steady-state studies. The results reported here are a representative sample of many reproducible runs which for lack of space cannot be included. In the text we will highlight these additional results when they deviate from the characteristic trends shown in the figures.

1. Temperature-Programmed Reaction (TPR) Studies.

Characteristic results obtained during TPR experiments are presented in Fig. 3. In these experiments, continuous monitoring of CO_2 production and surface temperature was combined with discrete FTIR sampling at 1-s intervals in an effort to record the dynamic behavior associated with ignition and quenching of the reaction.

The results in Fig. 3 were obtained with a flowing gas mixture of 9 cm^3/min CO, 5 cm^3/min O_2 (CO/O_2 = 1.8), and 220 cm^3/min of nitrogen. Figure 3a shows the gas (reactor) temperature which was programmed to increase approximately linearly for 1 h at 2.5°C per minute, reach a maximum at 315°C, and then decrease in a likewise manner. During TPR, dynamic response is simultaneously recorded for surface temperature (Fig. 3a), CO_2 production, and linear-bonded CO (Fig. 3b).

Initially, with the reactor at 165°C, the reaction rate is low and coverage of linear-bonded CO is high. In this region CO inhibition of oxygen chemisorption prevails and the reaction is essentially oxygen adsorption limited. As the temperature approaches 260°C, the reaction rate increases substantially with each additional degree. The surface temperature begins heating up faster than the reactor and the CO surface coverage decreases as temperature activation of CO desorption, surface reaction, and oxygen adsorption combine to increase the oxygen supply to the surface. At 265°C, these processes become autoaccelerating as ignition to a high steady state occurs with a simultaneous sudden change in CO_2,

surface CO, and surface temperature. The surface temperature is observed to spike through a 75°C maximum before becoming constant at about 40°C higher than the reactor temperature. The CO coverage suddenly decreases to near the detection limit which is in this case 1% coverage as calibrated through use of the quantitative relationship reported by Cant and Donaldson (*14*). CO_2 production increases to a maximum without overshoot where it remains constant beyond the ignition point. No change in reaction rate is observed through the programmed-temperature maximum. No further changes occur during cooling until the surface temperature again reaches the ignition temperature (285°C). At this point a marked change in the slope of the cooling curve for T_S is observed, accompanied by a detectable increase in the CO surface coverage and a discernible decreasing trend in CO_2 production. This delayed cooling of T_S occurs at a temperature where quenching would be expected if the process were symmetric aside from the obvious hysteresis caused by the elevated surface temperature. However, as reactor cooling continues, delayed cooling of the surface not only persists but also reverses and increases, reaching a local maximum in which T_S is 115°C higher than the reactor temperature. At the reversal point in T_S, the CO coverage suddenly begins to increase much more rapidly. As the maximum in T_S occurs, the CO_2 production has decreased to nearly one-half of its maximum value. Beyond its maximum, the surface temperature rapidly decreases concurrently with a decrease in CO_2 production and an increase in surface CO until the quenched reaction state is reached.

Other temperature-programming experiments obtained with CO/O_2 ratios as low as 0.32 show similar trends but less-pronounced surface temperature effects due to decreased reaction rates. Additional experiments show that the higher catalyst temperature can be observed as a steady state when the programming is completely halted in the reversal region, indicating that the catalyst overheating is not a transient resulting from the reaction programming. Under certain conditions, unstable and oscillatory behavior was observed during quenching in association with the region just prior to or just after the surface temperature reversal. Oscillatory CO surface coverage was also recorded in these cases. The nature of these oscillations will be presented in a subsequent paper.

Careful efforts were made to detect ir bands below 2000 cm^{-1} which would indicate a role of bridge-bonded CO. Weak bands at 1830 and 1940 cm^{-1} were observed at high steady-state conditions in which linear-bonded CO coverage was undetectable. Careful examination of this data lead to the conclusion, in agreement with the work of Kember and Sheppard (*15*), that both of these bands are a result of the higher catalyst temperature present during reaction. The same bands could always be obtained by comparing any two reference spectra taken in flowing nitrogen at temperatures differing by 50°C or more. This result lead to the conclusion that the infrared absorption properties of the support in the region 1800 to 2000 cm^{-1} are temperature sensitive. Thus the weak broad bands detected in this region cannot be identified with bridge-bonded CO, but can serve as an indication of large temperature gradients between the catalyst and the reactor gas phase.

2. *CO Concentration-Programmed Reaction (CO–CPR) Studies*

Carbon monoxide concentration-programming experiments were performed in an effort to ascertain the role of linear-bonded CO in the inhibition of the reaction rate. In each run, a fixed carrier gas, oxygen flow rate, and reactor temperature were used. During the experiment, the CO flow rate was increased linearly for a 2-h period and then decreased likewise for 2 h. For each run, discrete FTIR sampling was carried out by storing sets of 15 co-added

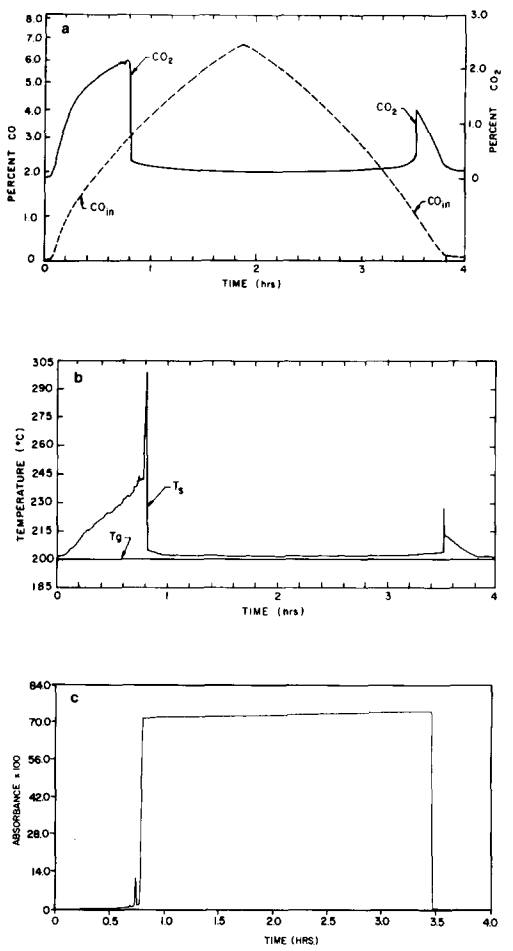

FIG. 4. Concentration programming of inlet CO with reactor at 200°C, 220 cm³/min N_2, 5 cm³/min O_2, and 13.5 cm³/min CO_{max}. (a) CO_{in}, and CO_2 production; (b) surface temperature response and constant reactor temperature; (c) spectragram showing response of linear-bonded CO.

scans in a total of 1000 scan sets. The surface temperature and outlet CO and CO_2 concentrations were also continuously monitored.

A representative example of CO–CPR is shown in Figs. 4a–c for a 200°C isothermal run. In this case, oxygen and nitrogen carrier flows were constant at 5.0 and 220 cm³/min, respectively, while the CO in the mixture was varied from zero to a maximum of 13.5 cm³/min. This run portrays the multiple steady-state and hysteresis behavior and the dynamic surface processes accompanying that behavior. The CO_2 production (Fig. 4a) is observed to increase through a maximum, followed by rapid quenching at a CO/O_2 ratio of 1.2. At this point a sudden increase in linear-bonded CO and surface temperature spike occurs simultaneously (Fig. 4b–c). The remarkable 55°C surface temperature spike shown here is apparently analogous to the temperature reversal during TPR. The brief spike in CO coverage just prior to quenching is a precursor to self-sustained oscillations which can be observed in this region. The hysteresis effect is clearly seen during the decreasing CO region as ignition does not occur until the CO/O_2 ratio drops to 0.4. During ignition, a marked surface temperature spike and disappearance of surface CO occur simultaneously and in an analogous manner to the ignition during TPR.

Similar CO–CPR experiments were performed at higher temperatures and higher oxygen concentrations to determine if a different dynamic behavior existed. In Fig. 5 we present results obtained for CO–CPR studies at 250°C and 300°C using 2.5 cm³/min O_2 and 220 cm³/min CO. These results indicate that the role of CO inhibition diminishes as the temperature increases. At 300°C (Fig. 5a) quenching does not occur when CO surface coverage increases rapidly at a CO/O_2 ratio of 1.7. Instead, a gradual inhibition occurs as CO is further increased. At 250°C (Fig. 5b), a partial quenching is observed in association with the rapid increase of CO surface coverage. While no surface temperature spike was observed at 300°C, it can be seen that at 250°C a spike occurs associated with an in proportion to the degree of quenching.

Additional CO–CPR experiments performed at 200°C indicate that increasing the amount of oxygen present decreases the surface temperature spike during quenching. An increase in oxygen flow to 7.5 cm³/min from the results in Fig. 4 produced os-

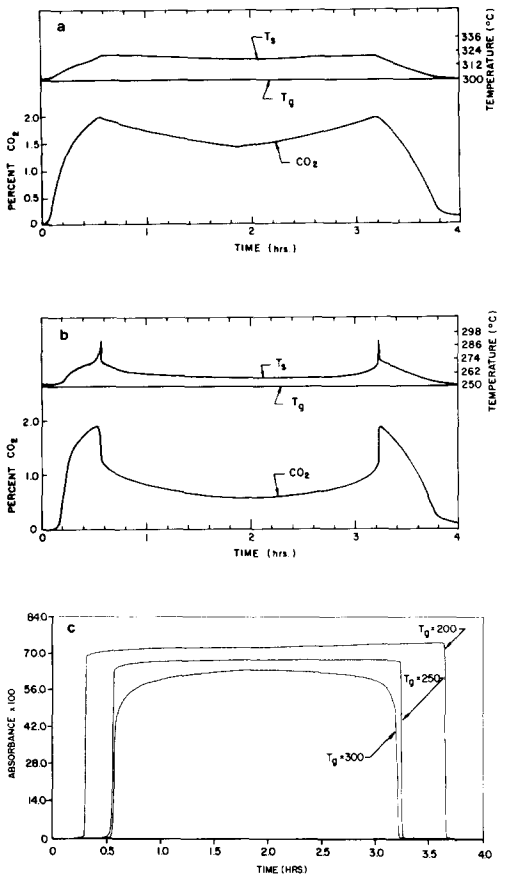

FIG. 5. Concentration programming of inlet CO at two different reactor temperatures and 220 cm³/min N_2, 2.5 cm³/min O_2, 0 to 13.5 cm³/min CO. (a) Response of T_S and CO_2 at 250°C; (b) response of T_S and CO_2 at 300°C; (c) spectragrams showing response of linear-bonded CO at each of three reactor temperatures.

cillatory surface dynamics during a lengthy quenching transition period. Further increase of the oxygen flow rate to 10 cm³/min resulted in the total disappearance of the surface temperature spike.

3. *Oxygen Concentration-Programmed Reaction (O_2–CPR Studies)*

The final dimension of the CO-oxidation dynamics was explored by programming oxygen as the independent variable. These experiments were carried out in the same manner as the CO–CPR results, but with the oxygen flow rate programmed to increase and then decrease while CO, N_2, and reactor temperature were held constant. An example of O_2–CPR carried out at 200°C is shown in Fig. 6. Nitrogen and CO flow rates were held constant at 200 and 9 cm³/min, respectively, while the oxygen flow rate was varied from zero to 28.5 cm³/min and back to zero again over a 3-h period.

These results are similar to the dynamic behavior observed during TPR. Ignition occurs at a CO/O_2 ratio of 0.4 producing temperature overshoots at the catalyst surface and rapid removal of CO coverage without an overshoot in CO_2 production. Once on the high-steady state branch, the surface temperature remained constant at 256°C. Throughout the region of high rates, the CO_2 concentration varied slightly with the changes in oxygen flow rate but the conversion remained constant at 90%. Upon decreasing the oxygen concentration a considerable hysteresis could be detected since the CO_2 production did not begin to decrease until the CO/O_2 ratio was 1.5. At this point adsorbed CO again became detectable by ir and steadily increased until quenching was complete. As had been observed in the corresponding region of the other programming experiments, a marked increase in the catalyst temperature was again indicated by the surface thermocouple.

Possible changes in the frequency of the ir absorption for linear-bonded CO was closely investigated for the results in Fig. 6 by obtaining data at 1-cm^{-1} spectral resolution instead of the 8-cm^{-1} resolution used in the previous experiments. The only variation observed was in the quenching region when the CO infrared peak first appeared at 2073 cm^{-1} and then increased to the normal 2078-cm^{-1} position at higher intensities. Similar changes at 3–5 cm^{-1} in the CO peak position have been recorded in other ir reaction studies on supported catalysts (*18*), while much larger variations apparently prevail for CO adsorption alone.

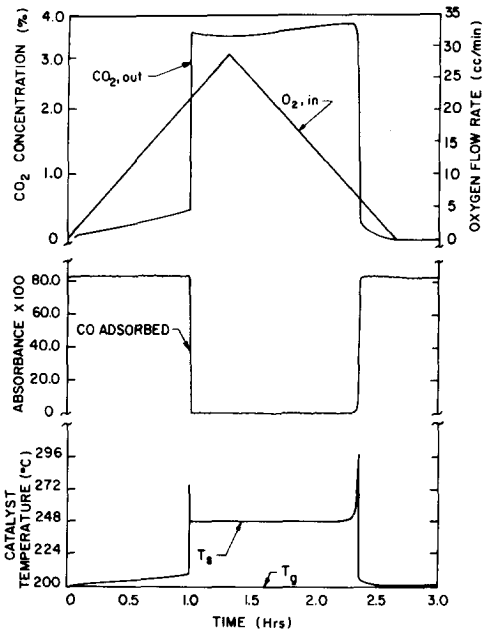

FIG. 6. Concentration programming of inlet oxygen flowrate (O_2–CPR) with reactor at 200°C, 200 cm³/min N_2, 9 cm³/min CO, and O_2 max of 28.5 cm³/min. (a) Indicates the programmed input of oxygen and the CO_2 production response; (b) surface temperature behavior during oxygen programming; (c) spectragram showing response of linear-bonded CO.

Additional experiments have been performed using different wafers, reactors, and experimental conditions to insure that our observations were indeed reproducible. A series of blank runs was conducted in which a pure SiO_2 wafer was tested under similar conditions of CO and temperature ramping. From the results of these runs, we concluded that neither the stainless-steel reactor walls, the aluminum sample holder, nor the Chromel–Alumel surface thermocouple were making detectable contributions to the catalytic activity. Also among our reproducibility tests was a single TPR experiment using a 2% Pd/ZSM5 zeolite in which a pronounced temperature reversal was also observed during quenching. These experiments prove that our results are not affected by extraneous factors, but rather, uncover a fundamental phenomena of importance to CO-oxidation on various high surface area supported catalysts.

We have also conducted tests to insure that our catalyst was operating in the kinetic regime using the method of diluting the catalyst with additional amounts of inert silica as proposed by Koros and Nowak (*16*). Others have found (*17, 18*) that internal mass transfer by diffusion is not rate-limiting under conditions similar to our own. However, in our case, the test was inconclusive because the catalyst shows a significant temperature rise during such experiments. As Koros and Nowak point out, a temperature rise inside the catalyst wafer may compensate for the effect of diffusion control, thereby making the test invalid.

DISCUSSION

Novel results obtained via the transient FTIR experiments used in this work have provided new insights into the complexities of the catalytic oxidation of CO on Pt/SiO_2. The following results related to the reaction mechanism were anticipated from previous studies by others (*18–23*) as well as by our own group (*24, 25*): (1) existence of multiple steady-state behavior, (2) reaction rate hysteresis, (3) CO inhibition at high concentration, (4) CO_2 production increases as CO coverage decreases, the later being below the detection limit of our instrument in the region of high steady state and CO/O_2 ratio less than stoichiometric. A second set of observations, apparently not reported before for this reaction, indicate the existence of a complex energy transfer process. These new findings include the following: (5) a rapid temperature overheating is observed during the ignition branch of the TPR experiments without concurrent overshoot in CO_2 production, (6) a surface temperature reversal and local maximum occurs during the cooling branch of the TPR experiments; (7) surface temperature overheating is observed concurrently with both reaction quenching and ignition during CO–

CPR. (8) O_2–CPR yields similar ignition and quenching phenomena as observed during TPR. In the following pages we will first, analyze the various possible interpretations and inferences that can be made from the ir data, followed by a tentative explanation of the inordinate overheating results.

The infrared data in Fig. 3–5 indicate that during high reaction rates and CO/O_2 ratio less than stoichiometry, CO coverage is lower than the 1% detectability limit of our instrument. While multiple steady-state and hysteresis behavior have been reported previously in the literature (*18–25*), our data indicates that this behavior disappears at 300°C. Furthermore, at this temperature a high rate of CO_2 production prevails in the presence of a rather high CO coverage which is not capable of quenching the reaction (Figs. 5a,c). Partial quenching is observed at 250°C (Fig. 5b) whereas complete quenching occurs at 200°C (Fig. 4). These results are difficult to reconcile with a L–H mechanism and, suggest at first, that an alternative reaction path via a modified Eley–Rideal mechanism (*26–28*), involving a short-lived adsorbed state might be operative. Such an intermediate would not be visible in the ir because it is not fully chemisorbed, which would explain our ir, TPR, and CPR results. However, Ertl and coworkers (*29*) have determined that at 442 K, under conditions of maximum oxygen coverage and high reaction rate, the surface residence time of CO adsorbed on Pt is no less than 6×10^{-4} s. This residence time indicates the participation of a fully chemisorbed CO (*29, 30*), and is sufficiently long for the adsorbed species to be detectable, provided that the coverage is above our detectability limit of 1%. In order to understand quantitatively the coverage level attained at high reaction rates, as well as the other results obtained, a theoretical simulation of our experimental results was carried out.

Details of the simulation are beyond the scope of this paper and will be the subject of a later publication. The model comprises transient surface site balances for CO and oxygen which include competitive CO and dissociative O_2 adsorption, CO desorption, and Langmuir–Hinshelwood (L–H) surface reaction of adsorbed CO and oxygen. Coverage dependent activation energies for CO desorption (*31, 32*) and L–H surface reaction taken from single crystal data (*29, 33*) were used. Also considered were mass and energy balances about the wafer, with film diffusion between bulk gases and the catalyst wafer. For simplicity, it was assumed that no intraphase gradients exist in the wafer and that the gas-phase concentration in the ir cell is well mixed. Numerical solution was carried out using our own experimental data and catalyst characteristics whenever possible.

Model results indicate that a L–H mechanism can account for many of the results shown in Figs. 3–5. High reaction rates can indeed occur between 200 and 300°C with very low CO coverages ($<10^{-3}$). Such low coverages are below our detectability limits and thus explain the absence of adsorbed CO at high steady states in our ir data. Model results also predict that at 300°C, high rates can be sustained in the presence of high CO coverage (90% of the maximum). This occurs because at this temperature the high rates of CO desorption and surface reaction provide enough empty sites for oxygen to dissociate and react. The model calculations also predict that near the stoichiometric point, inhibition occurs for increasing CO concentrations (Fig. 4), and hysteresis occurs following a subsequent decrease in CO concentrations.

While the model helped to resolve the question concerning the reaction mechanism, it failed to account for some of the new observations reported here regarding surface temperature. The model predicts higher surface temperatures as CO_2 production increases, but it does not account for the temperature spikes observed prior to CO–CPR and O_2–CPR quenching (Figs. 4

and 6) or the temperature reversal during TPR (Fig. 3). Furthermore, the model predicts that the temperature spike occurring during ignition (Fig. 3) is the result of burnoff of accumulated surface CO. Consequently the model results exhibit an overshoot in CO_2 production, which is contrary to the experimental observation.

The model was modified to include the heat of chemisorption of CO (28–34 kcal/mole) (*31, 32, 34*) as a possible source for the temperature increase during quenching. Calculations quickly showed that CO accumulation up to monolayer coverage could not produce the inordinate temperature effects observed. A further modification was introduced into the model by assuming that an inactive platinum oxide species would form in an oxygen-rich environment and would be reduced as quenching occurs due to high CO coverage (*35–38*). Although this model produced oscillatory behavior, the exothermic reduction of the surface oxide was also found to be an inadequate source for the observed surface heating effects.

The inordinate temperature excursions that occur during ignition and quenching without a concurrent overshoot in CO_2 production cannot be easily explained if our system is considered to be as ideal as our model. Several factors might contribute to create nonideal conditions leading to complex energy transfer mechanisms. Each of these factors is discussed below, although at this writing we cannot unambiguously identify the cause of the observed results.

The major simplifying assumptions made in the model are that the gas phase is well mixed, and that the concentrations and temperatures inside the wafer are uniform throughout. The high conversions induced by the TPR and CPR experiments may actually be leading to gradients along the reactor which might cause local gradients in the wafer. For example, the area of the wafer near the reactor inlet could be at a higher concentration than the portion of the wafer nearest the outlet. Such gradients might lead to concentration profiles along the wafer which resemble the profiles in a fixed bed rather than a well-mixed system. If this is the case, concentration and temperature waves propagating along the wafer could lead to the unstable behavior observed prior to and after the temperature reversal. Such behavior has been documented and analyzed by Wicke (*39*) and Hlavacek (*40*) to explain self-sustained oscillations in a fixed-bed reactor.

Another important assumption made in the model is that the surface temperatures are uniform throughout the wafer. This might not be so, since the possible existence of concentration gradients can certainly lead to temperature gradients and vice versa. Furthermore, recent work by Schmitz and co-workers (*41*) using infrared thermography during H_2 oxidation on one of our own 5 wt% Pt/SiO_2 wafers has shown that certain areas of the catalyst are hotter than others. This phenomena may be due to poor thermal communication between the particles within the catalyst wafer or to nonuniformities in the wafer density and cannot be excluded from our results.

While the presence of gradients and thermal nonuniformities in the wafer could be responsible in part for the observations reported here, other energy transport processes could also contribute to the results. For example, a common feature of the temperature excursions is that they occur only when the CO (and oxygen) coverage is changing between its high and low limits. Recently, several papers have reported on the formation of hot CO_2 molecules on Pt single crystals and polycrystalline Pt foils (*29, 30, 33, 42–45*). Ertl and co-workers (*33*) have shown that the extent of energy transfer between nascent CO_2 and a Pt surface (or thermal accommodation) depends on the surface temperature and on the coverage of CO and oxygen. These authors found that thermal accommodation is

nearly complete for reaction on the small fraction of surface defect sites due to their high adsorption energy. The majority of surface sites, however, have lower adsorption energy which can lead to the desorption of nascent CO_2 molecules having excess translational and internal energy. During reacting conditions, high surface temperature or predominant coverage by either reactant was shown to favor the formation of hot CO_2. At intermediate temperatures, however, a significant increase in thermal accommodation was observed when the total coverage of both reactants became low, such as during the switch from predominant coverage by one reactant to predominant coverage by the other. The authors propose that at low total coverage, the reaction preferentially occurs at the sites of higher adsorption energy because the oxygen sticking coefficient is significantly greater on these sites than for the lower adsorption energy sites.

These results, obtained on single-crystal catalysts at UHV conditions might not be applicable to our catalysts, yet the similarity between coverage and temperature dependence for hot CO_2 production have led us to speculate that this process might have a bearing on the results. We propose that if these hot CO_2 molecules are formed in our system, they might remove energy from the Pt crystallites and transfer it to the diluent gas to be transported out of the wafer by diffusion. This energy transport mechanism would remove part of the heat of reaction from the wafer providing an additional cooling process that reduces the catalyst temperature from its maximum value. The formation of hot CO_2 and thus the additional cooling would be manifest at low CO coverage where the oxygen coverage is high. Thus, changes from high oxygen to high CO coverage during quenching might lead to the disappearance of the cooling effect due to higher thermal accommodation during the coverage switch. This could result in an apparent overheating during quenching, even when CO_2 production is actually decreasing.

High-resolution ir spectra of CO_2 produced at high steady state did not show changes in the vibrational and rotational energy levels of the CO_2 molecules, thus apparently not supporting this explanation. However, since hot CO_2 molecules will collide and transfer energy to the N_2 diluent, the lifetime of the excited states of CO_2 would be too short to allow detection in our system, thus neither proving or disproving this hypothesis. The possible presence of gradients and their effect on the results does not permit discrimination among all these factors, and the proposed cooling mechanism via hot CO_2 is speculative at this time. Further work to eliminate gradients and to measure the temperature distribution throughout the catalyst is underway to determine the influence of the factors referred to above in our results.

It is important to realize that temperature excursions reported here might not be apparent in systems where less-sensitive thermocouples are used or when other catalyst supports are used. It is interesting to note that the bimodal pore size distribution and low thermal conductivity of our SiO_2 support combined with the high heat of reaction provides a setting in which the largest deviations from isothermal behavior are likely to occur (*46*). In addition the bulk diffusion of intraphase gases in the macropores should be expected to contribute to heat removal from such a catalyst.

While the hypotheses offered here to explain our data are at this point speculative, the results presented in this paper clearly show that CO oxidation on Pt/SiO_2 is a complex process involving transport of mass and energy between the metal crystallites, the catalyst support, and intraphase and bulk gases. It is encouraging to note that, when surface temperatures and concentrations are *carefully* measured on sup-

ported catalysts, as presented in this work, certain aspects of the behavior recorded on single crystals might be relevant to supported catalysts.

ACKNOWLEDGMENTS

Professor G. Ertl (U. of Munich) has kindly sent us a manuscript not yet publicly available (Ref. (*33*)). Girish Chitnis (present address: Union Carbide Corporation, Charleston, West Virginia) designed the reactor. Dave Ramsey (present address: General Electric Corporation, Gainesville, Florida) did the construction and preliminary testing. Funds for the FTIR spectrometer were provided by NSF Equipment Grant ENG 79-11459. Graduate student support was provided by the Industrial Waste Elimination Research Center (IWERC-IIT/Notre Dame) funded by EPA.

REFERENCES

1. Eischens, R. P., *in* "The Surface Chemistry of Metals and Semiconductors" (H. C. Gatos, Ed.). Wiley, New York, 1959.
2. Hair, M. L., "Infrared Spectroscopy in Surface Chemistry." Dekker, New York, 1967.
3. Delgass, W. N., Haller, G. L., Kellerman, R., and Lunsford, J. H., "Spectroscopy in Heterogeneous Catalysis." Academic Press, New York, 1979.
4. Bell, A. T., and Hair, M. L., "Vibrational Spectroscopies for Adsorbed Species," ACS Symposium Series, Vol. 137. Amer. Chem. Soc., Washington, D.C., 1980.
5. Kobayashi, H., and Kobayashi, M., *Catal. Rev.-Sci. Eng.* **10,** 139 (1974).
6. Bennett, C. O., *Catal. Rev.-Sci. Eng.* **13,** 121 (1976).
7. Tamaru, K., "Dynamic Heterogeneous Catalysis." Academic Press, New York, 1978.
8. Hegedus, L. L., and Oh, S. H., ACS Symposium Series, Vol. 178, p. 76. Amer. Chem. Soc., Washington, D.C., 1982.
9. Hicks, R. F., Kellner, C. S., Savotsky, B. J., Hecker, W. C., and Bell, A. T., *J. Catal.* **71,** 216 (1981).
10. Vannice, M. A., Moon, S. H., Twu, C. C., and Wang, S-Y., *J. Phys. E* **12,** 849 (1979).
11. Gonzalez, R. D., and Miura, H., *J. Phys. E* **15,** 373 (1982).
12. Sheintuch, M., and Schmitz, R. A., *Catal. Rev.-Sci. Eng.* **15,** 107 (1977).
13. Engel, T., and Ertl, G., "Advances in Catalysis," Vol. 28, p. 1. Academic Press, New York, 1979.
14. Cant, N. W., and Donaldson, R. A., *J. Catal.* **178,** 461 (1982).
15. Kember, D. R., and Sheppard, N., *J. Chem. Soc., Faraday Trans. 2* 77, 1321 (1981).
16. Koros, R. M., and Nowak, E. J., *Chem. Eng. Sci.* **22,** 470 (1967).
17. Herz, R. K., Kiela, J. B., and Marin, S. P., *J. Catal.* **73,** 66 (1982).
18. Haaland, D. M., and Williams, F. L., *J. Catal.* **76,** 450 (1982).
19. Wicke, E., Kummann, P., Keil, W., and Schiefler, J., *Ber. Bunsenges. Phys. Chem.* **84,** 315 (1980).
20. Dwyer, S. M., and Bennett, C. O., *J. Catal.* **75,** 275 (1982).
21. Goodman, M. G., Cutlip, M. B., Kenney, C. N., Morton, W., and Mukesh, D., *Surf. Sci.* **120,** L453 (1982).
22. Sarkany, J., Bartok, M., and Gonzalez, R. D., *J. Catal.* **81,** 347 (1983).
23. McCarthy, F., Zahradnik, J., Kuczynski, G. C., and Carberry, J. J., *J. Catal.* **39,** 29 (1975).
24. Varghese, P., Carberry, J. J., and Wolf, E. E., *J. Catal.* **55,** 76 (1978).
25. Liao, P. C., and Wolf, E. E., *Chem. Eng. Commun.* **13,** 315 (1982).
25a. Norton, P. R., Davies, J. A., Creber, D. K., Sitter, C. W., and Jackman, T. E., *Surf. Sci.* **108,** 205 (1981).
25b. Ertl, G., Norton, P. R., and Rustig, J., *Phys. Rev. Lett.* **49** (2), 177 (1982).
26. Alnot, M., Fusy, J., and Cassuto, A., *Surf. Sci.* **57,** 651 (1976).
27. Harris, J., and Kasemo, B., *Surf. Sci.* **105,** L281 (1981).
28. White, J. M., and Golchet, A., *J. Chem. Phys.* **66** (12), 5744 (1977).
29. Campbell, C. T., Ertl, G., Kuipers, H., and Segner, J., *J. Chem. Phys.* **73** (11), 5862 (1980).
30. Ertl, G., *Ber. Bunsenges. Phys. Chem.* **86,** 425 (1982).
31. McCabe, R. W., and Schmidt, L. D., *Surf. Sci.* **66,** 101 (1977).
32. Campbell, C. T., Ertl, G., Kuipers, H., and Segner, J., *Surf. Sci.* **107,** 207 (1981).
33. Segner, J., Campbell, C. T., Doyen, G., and Ertl, G., *Surf. Sci.*, in press.
34. Weinberg, W. H., and Merrill, R. P., *J. Catal.* **40,** 268 (1975).
35. Berry, R. J., *Surf. Sci.* **76,** 415 (1978).
36. Suhl, H., *Surf. Sci.* **107,** 88 (1981).
37. Vayenas, C. G., and Michaels, J. N., *Surf. Sci.* **120,** L405 (1982).
38. Sales, B. C., Turner, J. E., and Maple, M. B., *Surf. Sci.* **112,** 272 (1981).
39. Padberg, G., and Wicke, E., *Chem. Eng. Sci.* **22,** 1035 (1967).
40. Puszynski, J., and Hlavacek, V., *Chem. Eng. Sci.* **35,** 1769 (1980).
41. Schmitz, R. A., D'Netto, G. A., Razon, L. F., and Brown, J. R., "Proceedings, NATO Workshop on Chemical Instabilities." Austin, Texas (1983).

42. Engel, T. and Ertl, G., *in* "The Chemical Physics of Solid Surfaces and Heterogeneous Catalysis" (D. A. King, Ed.), Vol. 4, pp. 73–93. Elsevier, New York, 1982.
43. Becker, C. A., Cowin, J. P., Wharton, L., and Auerbach, D. J., *J. Chem. Phys.* **67,** 3394 (1977).
44. Mantell, D. A., Ryali, S. B., Halpern, B. L., Haller, G. L., and Fenn, J. B., *Chem. Phys. Lett.* **81** (2), 185 (1981).
45. Beranasek, S. L., and Leone, S. R., *Chem. Phys. Lett.* **84,** 401 (1981).
46. Satterfield, C. N., and Sherwood, T. K., "The Role of Diffusion in Catalysis." Addison-Wesley, Reading, Mass., 1963.